ACS Infectious Diseases

pubs.acs.org/journal/aidcbc

Article

Virus-Like Particles of SARS-CoV-2 as Virus Surrogates: Morphology, Immunogenicity, and Internalization in Neuronal Cells

Chandra Shekhar Kumar, Balwant Singh, Zaigham Abbas Rizvi, Hilal Ahmad Parray, Jitender Kumar Verma, Sukanya Ghosh,[‖] Amitabha Mukhopadhyay, Amit Awasthi, Tripti Shrivastava, and Manidipa Banerjee*

Cite This: https://doi.org/10.1021/acsinfecdis.2c00217

Read Online

ACCESS | Metrics & More | Article Recommendations | Supporting Information

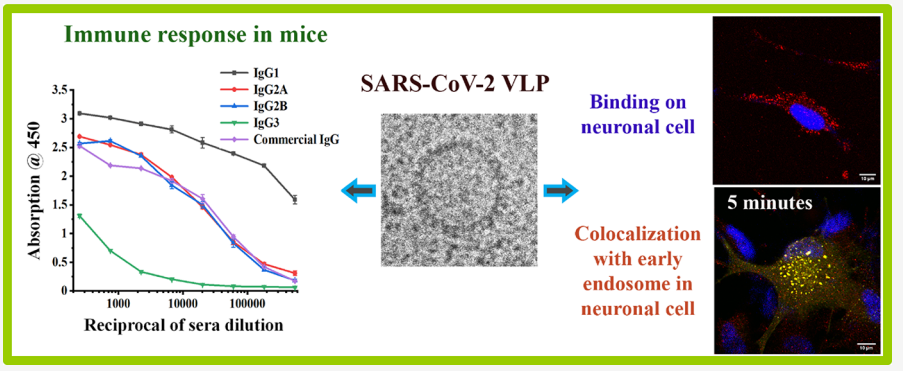

ABSTRACT: The engineering of virus-like particles (VLPs) is a viable strategy for the development of vaccines and for the identification of therapeutic targets without using live viruses. Here, we report the generation and characterization of quadruple-antigen SARS-CoV-2 VLPs. VLPs were generated by transient transfection of two expression cassettes in adherent HEK293T cells—one cassette containing M^{pro} for processing of three structural proteins (M, E, and N), and the second cassette expressing the Spike protein. Further characterization revealed that the VLPs retain close morphological and antigenic similarity with the native virus and also bind strongly to the SARS-CoV-2 receptor hACE-2 in an *in vitro* binding assay. Interestingly, the VLPs were found to internalize into U87-MG cells through cholesterol-rich domains in a dynamin-dependent process. Finally, our results showed that mice immunized with VLPs induce robust humoral and cellular immune responses mediated by enhanced levels of IL-4, IL-17, and IFNγ. Taken together, our results demonstrate that VLPs mimic the native virus and induce a strong immune response, indicating the possible use of these particles as an alternative vaccine candidate against SARS-CoV-2. VLPs can also be effective in mapping the initial stages of virus entry and screening inhibitors.

KEYWORDS: *SARS-CoV-2, virus-like particles, morphology, antigenicity, U87-MG cells*

The pandemic caused by the novel β-coronavirus SARS-CoV-2 has triggered an unprecedented health emergency globally.[1] The efforts to develop or repurpose therapeutic molecules against the virus have seen limited success.[2−6] Two LNP-stabilized mRNA vaccines, as well as inactivated virus and chimeric virus-based vaccines, have been utilized for mass vaccination worldwide.[2,3,7−11] Additionally, several types of vaccine formulations, including inactivated virus, purified surface glycoprotein, and chimeric, replicating, or non-replicating viruses are approved or are in different phases of clinical trials.

Virus-like particles (VLPs) are known as safe and efficacious alternatives to natural viruses as they are non-infectious particles with a multivalent and native-like display of surface antigens.[12] VLPs are a safer alternative to inactivated or attenuated viruses for vaccination[12] as demonstrated by global usage of Cervarix and Gardasil, HPV VLP-based vaccines against cervical cancer.[13] VLPs are also powerful biochemical tools as they can be utilized to understand the architecture, assembly, and various stages of host interaction by highly pathogenic viruses at relatively lower biosafety level facilities. Several methods to generate native-like or chimeric VLPs of β-coronaviruses have been reported.[14−20] The BSL-3 categorization of SARS-CoV-2 makes the biochemical investigation into the viral life cycle challenging, and native VLPs have

Received: April 23, 2022

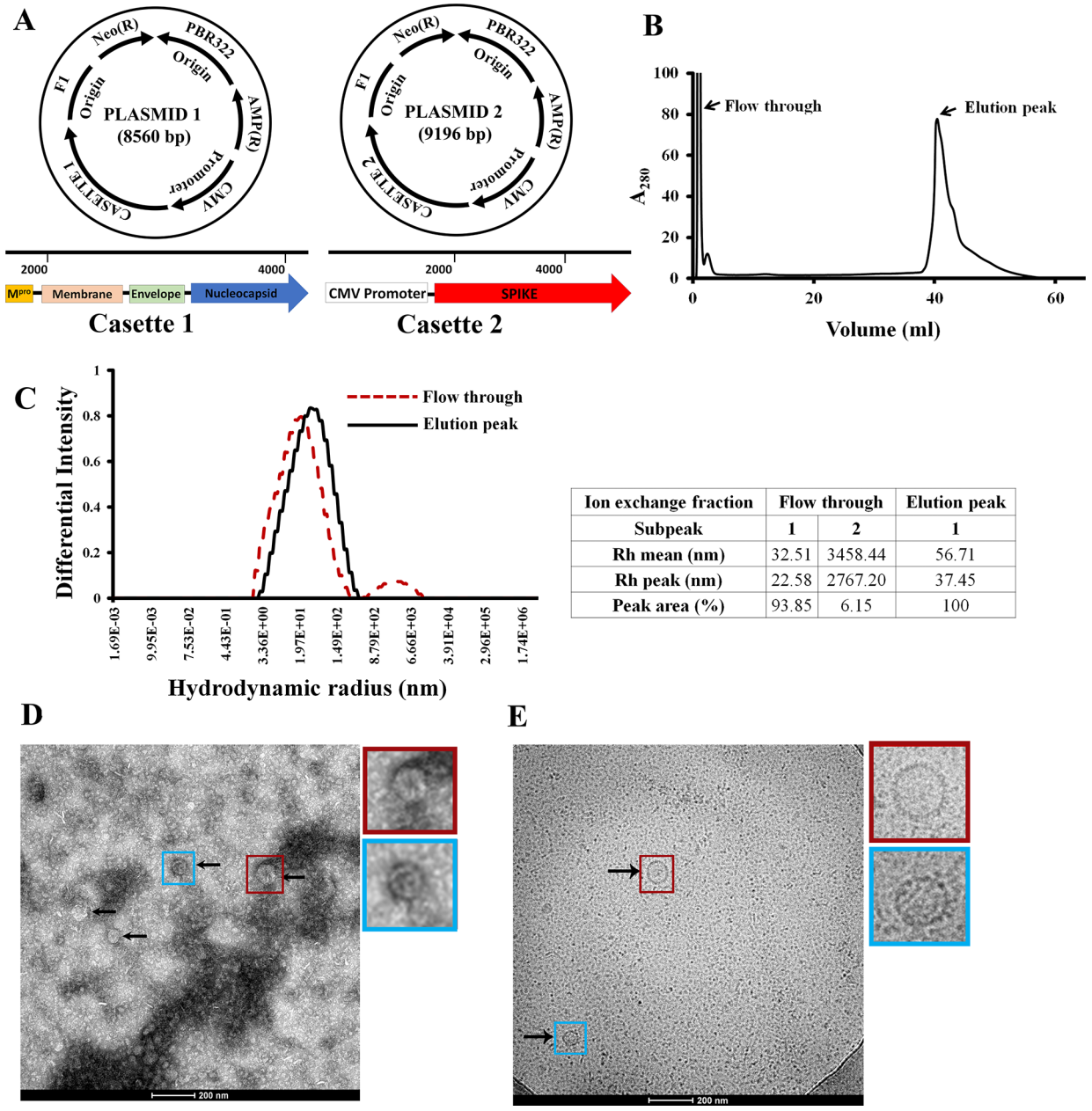

Ion exchange fraction	Flow through		Elution peak
Subpeak	1	2	1
Rh mean (nm)	32.51	3458.44	56.71
Rh peak (nm)	22.58	2767.20	37.45
Peak area (%)	93.85	6.15	100

Figure 1. Production strategy, purification, and morphological characterization of SARS-CoV-2 VLPs. (A) Schematic of expression vectors used to generate SARS-CoV-2 virus-like particles. (B) Purification profile in anion exchange chromatography. (C) Dynamic light scattering (DLS) of the flow-through (dotted line) and elution peaks (solid line). The Rh_{mean} of the peaks is indicated in tabular form. (D) Negative stain and (E) cryoelectron micrographs of the VLPs.

excellent potential as an approachable alternative for such studies.[21]

Co-expression of the structural proteins Membrane (M) and Envelope (E) is the fundamental requirement for β-coronavirus particle assembly, while the addition of the Spike (S) protein results in the generation of VLPs that resemble native virions.[14] M is the most abundant component of the virus envelope, which directs the assembly of coronaviruses through interactions with all other structural proteins.[22] E is a small membrane protein or "viroporin" that is thought to promote the budding of virus particles by pinching off cellular membrane surfaces.[23] S is a class I fusion protein that mediates attachment of SARS-CoV-2 to the major cell surface receptor human angiotensin-converting enzyme 2 (ACE2).[24−27] S also interacts with a secondary receptor, neuropilin-1, to mediate virus entry in respiratory and olfactory cells.[28,29] Due to its exposed conformation on the surface of the virus, S is highly immunogenic and is the main focus of current vaccine development.[3] N packages the RNA genome to form the nucleocapsid and has also been shown to be highly immunogenic.[30,31] While N is not necessarily required for envelope formation,[14] it appears to play an important role in the assembly and stability of the complete virion and in the enhancement of VLP yields.[32]

In this work, we generated a VLP containing all four major structural proteins—S, M, E, and N—as the closest mimic of SARS-CoV-2. The structural proteins S, M, and N are known to individually trigger robust T-cell-mediated immune response.[33−37] VLPs were generated by transient transfection in a mammalian expression system, which produces the most

https://doi.org/10.1021/acsinfecdis.2c00217
ACS Infect. Dis. XXXX, XXX, XXX−XXX

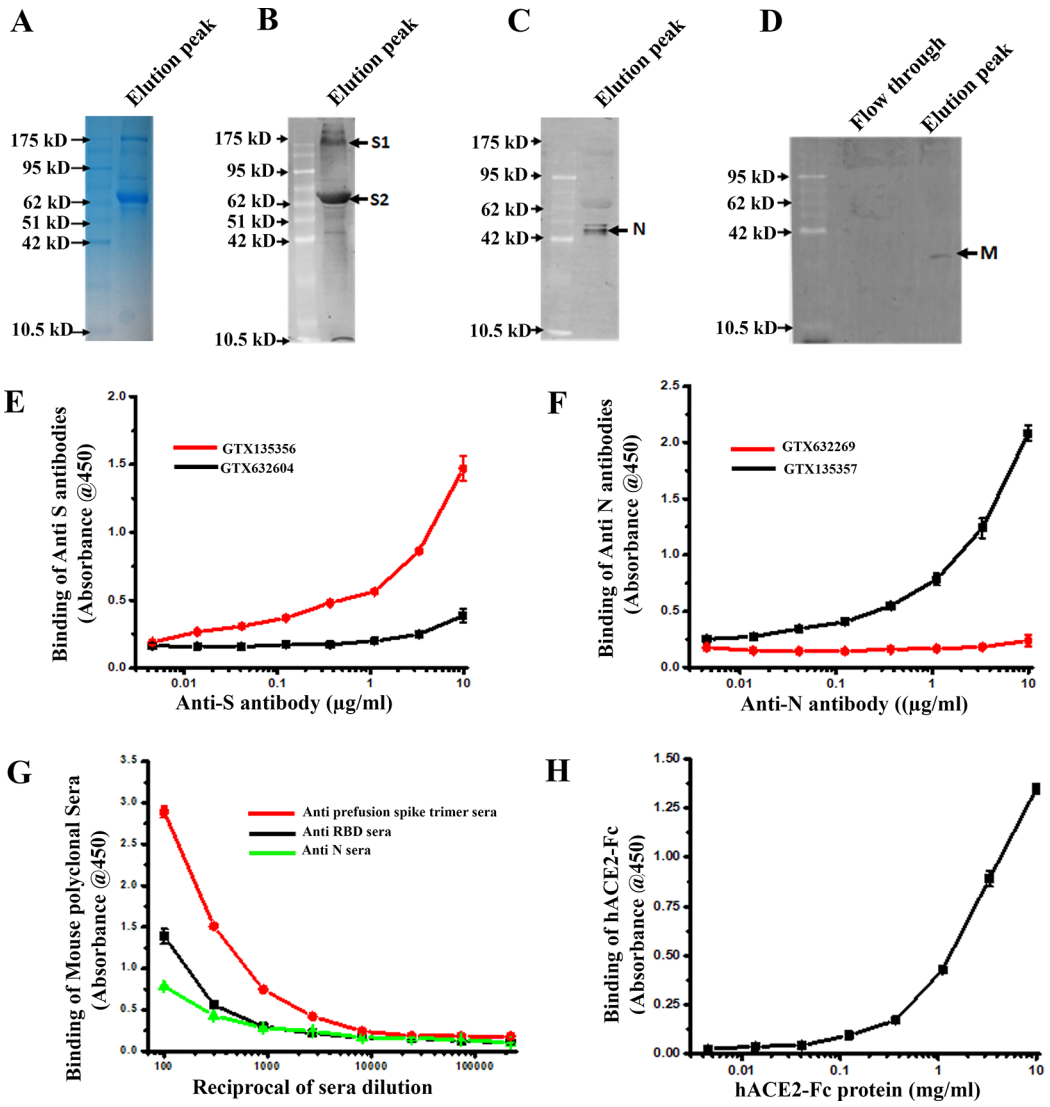

Figure 2. Antigenic characterization of SARS-CoV-2 VLPs. (A) SDS-PAGE analysis of purified VLPs. (B–D) Western blots with anti-S, anti-N, and anti-M antibodies, respectively. (D) A Western blot with an anti-M antibody has been carried out for both the flow through and elution fractions from ion-exchange chromatography. (E–G) ELISA-based analysis of SARS-CoV-2 VLP binding to (E) commercial anti-S, (F) anti-N antibodies, and (G) mouse polyclonal sera. (H) Binding profile of VLPs to the SARS-CoV-2 receptor hACE2-Fc.

faithful post-translational modifications (PTM). Our strategy for generating VLPs relied on the main viral protease (M^{pro}) to proteolytically cleave M, E, and N from a pre-protein, while S was co-expressed from a separate vector. The VLPs displayed native virus-like morphology, cross-reactivity with a variety of antibodies and antisera against structural proteins, and the ability to internalize in neuronal cells and elicited a robust humoral and cellular immune response in mice. We demonstrate that these VLPs can be effective as vaccine candidates and can also be utilized effectively as virus surrogates for studying the early stages of host–virus interaction.

RESULTS

SARS-CoV-2 VLP Generation and Morphological Characterization. For generating SARS-CoV-2 VLPs, the structural proteins S, N, M, and E were co-expressed in adherent HEK293T cells from two different plasmids as described in the Methods section. The monocistronic cassette utilized for the expression of M, E, and N (Figure 1A) also contained the cDNA for the main viral protease M^{pro} for proteolytic processing of the pre-protein. An optimized cleavage site for M^{pro} (SAVLQ ↓ SGFRK) was included between the cDNA sequences corresponding to each protein. The sequences for the structural proteins were sourced from the Wuhan-Hu-1 SARS-CoV-2 isolate (NCBI reference sequence: NC_045512.2), and codon-optimized for expression in mammalian cells. VLPs were purified from the culture media 72 h post-transfection by ultracentrifugation and anion exchange chromatography as described. In anion exchange chromatography, a large flow-through peak was initially observed, which was followed by an elution peak at a NaCl concentration of ∼600 mM. This pattern was consistently observed with multiple VLP preparations (Figure 1B).

For size-based characterization of the fractions from anion exchange chromatography, dynamic light scattering (DLS) was used. While the flow through showed the presence of multiple peaks with a range of hydrodynamic radii (Rh_{mean}), analysis of the elution peak indicated the presence of a relatively compact species (Figure 1C) with an Rh_{mean} of 56.71 nm. The contents

https://doi.org/10.1021/acsinfecdis.2c00217
ACS Infect. Dis. XXXX, XXX, XXX–XXX

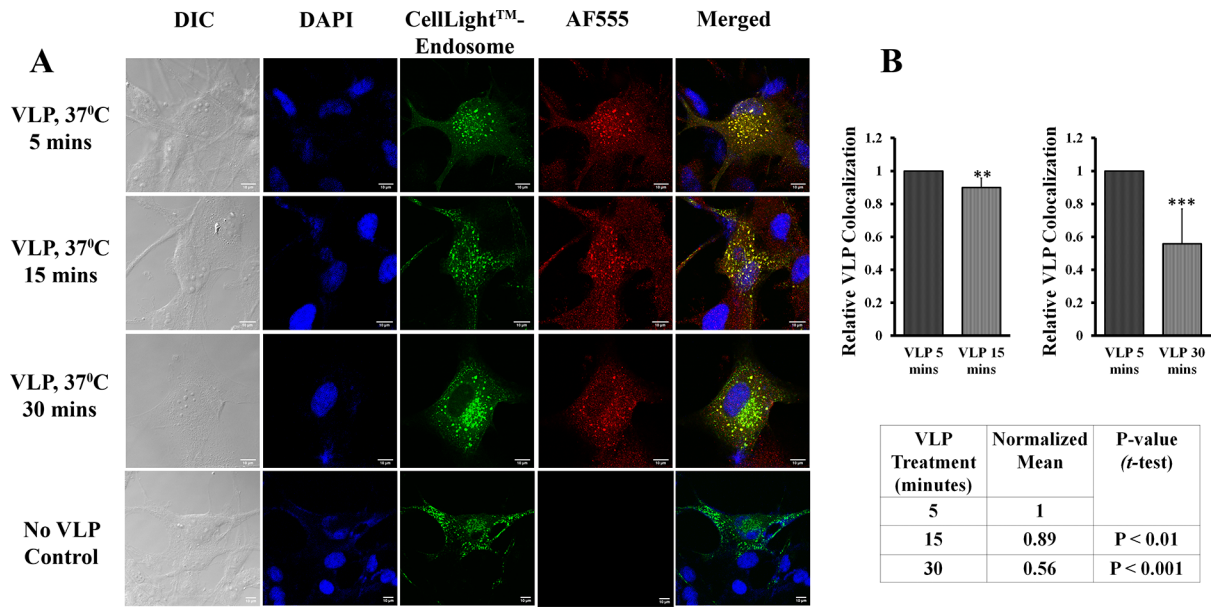

VLP Treatment (minutes)	Normalized Mean	P-value (*t*-test)
5	1	
15	0.89	P < 0.01
30	0.56	P < 0.001

Figure 3. Entry of SARS-CoV-2 VLPs in U87-MG cells and accumulation in early endosomes. (A) Nuclei in U87-MG cells are stained with DAPI (blue), endosomal compartments are stained with CellLight-GFP reagent (green), and VLPs are stained with Alexa-555 in conjunction with an anti-S polyclonal antibody (red). Time points of 5, 15, and 30 min following the association of U87-MG cells with VLPs at 37 °C were analyzed. U87-MG cells with no VLP treatment were used as a control. All images are at 63× magnification, (scale bar, 10 μm). (B) Relative colocalization of VLPs with early endosomes in U87-MG cells at 37 degrees for 5, 15, and 30 min. Colocalization values averaged from 10 images per sample were normalized against the highest value for semi-quantification. A two-paired Student's *t* test was performed to statistically compare the colocalization of VLPs with the early endosomes at 5, 15, and 30 min post VLP treatment in U87-MG cells. The statistically significant values are denoted by $^{**}P < 0.01$ and $^{***}P < 0.001$.

of the elution peak were visualized using electron microscopy. Negative-stain electron microscopy showed the presence of particles with diameters ranging from 80 to 120 nm (Figure 1D), while cryoelectron microscopy showed the presence of relatively circular particles (Figure 1E), with the typical brush-like pattern of Spike proteins clearly visible on the surface of particles at higher magnifications.

Antigenic Characterization of the VLPs. Purified VLPs were analyzed using SDS-PAGE and Western blotting with antibodies against SARS-CoV-2 Spike, Nucleocapsid, and Membrane proteins (Figure 2A–D). The anti-Spike polyclonal antibody detected prominent bands at ∼175 KD and ∼ 65 KD, consistent with the molecular weight of the intact spike protein and S1/S2 fragments,[38,39] along with other lower-molecular weight bands (Figure 2B). A polyclonal antibody against the nucleocapsid protein detected a band at the expected molecular weight of 46 KD[40] (Figure 2C). Similar molecular weight bands cross-reacting with the anti-spike and nucleocapsid antibodies were also detected in the flow-through peak (data not shown). A polyclonal antibody against the membrane protein of SARS-CoV was utilized for the detection of M (Figure 2D). Interestingly, only the elution peak showed cross-reactivity with this antibody, with the detection of a band of the expected size (∼ 24 KD).[41] No corresponding band was detected in the flow-through peak (Figure 2D). This suggests that the elution peak probably contains correctly formed SARS-CoV-2 VLPs, while the flow through likely consisted of aggregates of multiple structural proteins.

To ensure native virus-like conformation of structural proteins on the surface of VLPs, the antigenicity of the VLPs against a variety of anti-S and anti-N antibodies was tested using ELISA-based assays. The particles showed relatively higher binding to a polyclonal antibody against the S1 domain of the SARS-CoV-2 Spike protein (GeneTex GTX135356), compared to a monoclonal antibody (GTX632604) against a small region (amino acids 1029–1192) of the S2 domain (Figure 2E). Since the S1 domain is more exposed on the surface of virus particles compared to the S2 domain, the relatively higher binding of VLPs to GTX135356 indicates a native-like conformation and organization of Spike proteins on the surface of VLPs. Likewise, VLPs showed that substantial binding to a polyclonal antibody against the whole nucleocapsid (GeneTex GTX135357) while binding to a monoclonal antibody against amino acids 121–422 of the nucleocapsid (GeneTex GTX632269), which is less exposed, was almost negligible (Figure 2F). A similar, conformation-dependent binding to construct-specific polyclonal antisera was detected. VLPs showed maximum binding to antisera against trimeric spike prefusion forms (S2P), followed by the anti-receptor binding domain (RBD) and anti-nucleoprotein antisera (Figure 2G). This pattern of enhanced binding to exposed components on the virus surface indicated the morphological similarity of the VLPs to native SARS-CoV-2 virions. The correct conformation of Spike was further substantiated by the high affinity of the VLPs against the SARS-CoV-2 receptor, human angiotensin-converting enzyme 2 (hACE2) in conjunction with IgG (Figure 2H). The ELISA platform indicated that ACE2-Fc bound to the SARS-CoV-2 VLPs with an EC_{50} of 2.310 μg/mL, which is comparable with previously reported values.[42]

Entry of SARS-CoV-2 VLPs in U87MG Cells. The ability of SARS-CoV-2 VLPs to bind and enter the glioblastoma cell line U87-MG was tested. Human coronaviruses are known to invade the central nervous system (CNS) through olfactory nerve fibers or other routes, resulting in neuronal cell death and neurological symptoms,[43] and SARS-CoV-2 has been

https://doi.org/10.1021/acsinfecdis.2c00217
ACS Infect. Dis. XXXX, XXX, XXX−XXX

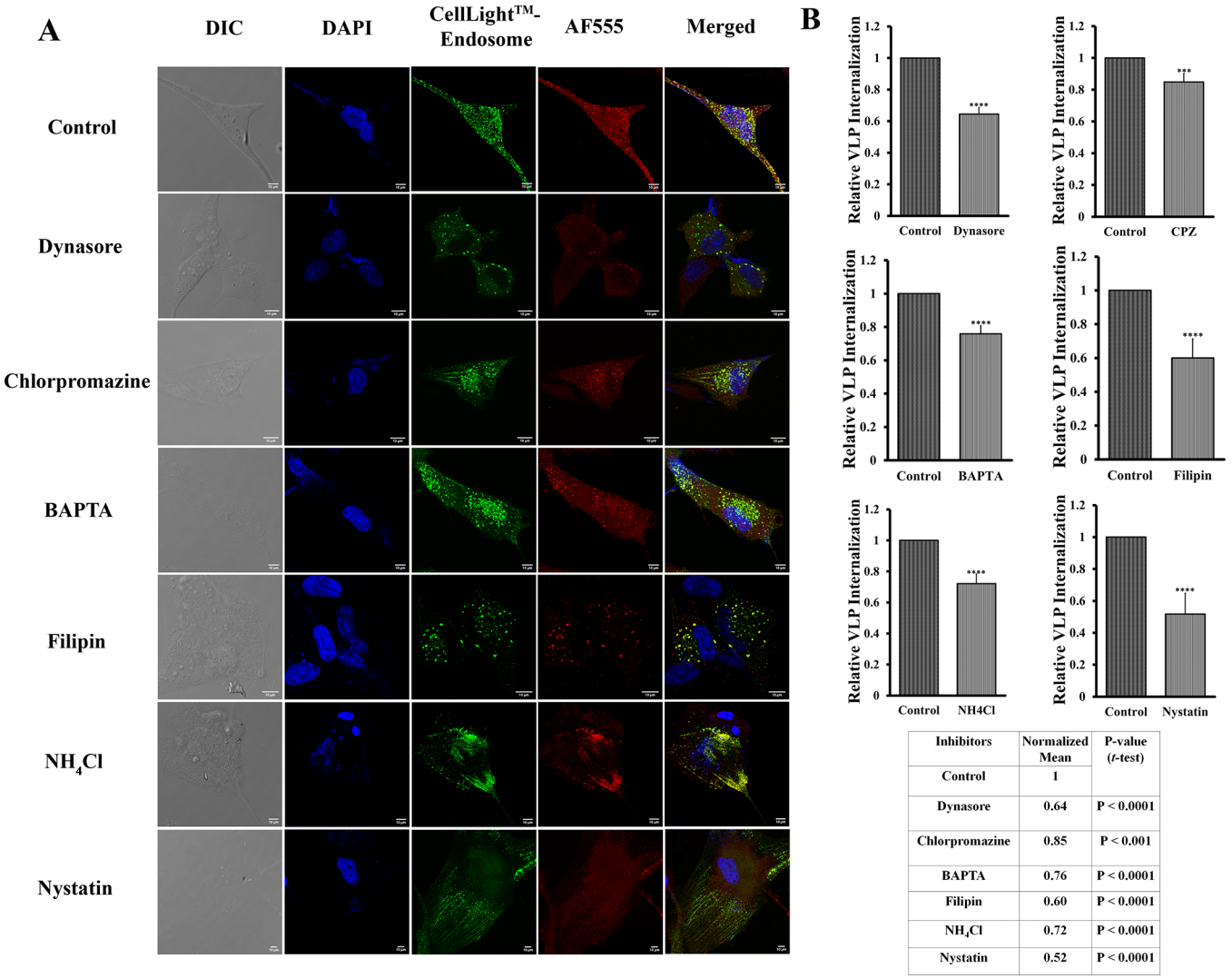

Inhibitors	Normalized Mean	P-value (*t*-test)
Control	1	
Dynasore	0.64	P < 0.0001
Chlorpromazine	0.85	P < 0.001
BAPTA	0.76	P < 0.0001
Filipin	0.60	P < 0.0001
NH_4Cl	0.72	P < 0.0001
Nystatin	0.52	P < 0.0001

Figure 4. Effect of inhibitors on the early endosomal accumulation of SARS-CoV-2 VLPs in neuronal cells. (A) Nuclei in U87-MG cells are stained with DAPI (blue), endosomal compartments are stained with CellLight-GFP reagent (green), and VLPs are stained with Alexa-555 in conjunction with an anti-S polyclonal antibody (red). The effect on the colocalization of VLPs with early endosomal marker was determined upon pretreatment of U87-MG cells with dynasore (80 μM), chlorpromazine (10 μM), BAPTA (25 μM), filipin (1 μM), NH_4Cl (50 mM), and nystatin (20 μg/mL). All images are at 63× magnification, (scale bar, 10 μm). (B) Relative colocalization of VLPs with early endosomes in presence of various inhibitors. Colocalization values averaged from 10 images per sample were normalized against the highest value (no inhibitor added) for semi-quantification. A two-tailed Student's *t* test was performed to compare the control with inhibitor-treated cells. The statistically significant values are denoted by ***$P < 0.001$ and ****$P < 0.0001$.

shown to invade and replicate in neuronal glioblastoma cells.[44] For monitoring cell surface binding, purified VLPs (12 μg of total protein) were added to U87-MG cells for 1 h at 4 °C, and the Spike protein associated with the VLPs was detected using an anti-SARS-CoV-2 Spike antibody in conjunction with an Alexa Fluor 555-labeled secondary antibody. Association of the VLPs with HEK293T cells was also monitored as a control. While the VLPs showed negligible binding to HEK293T cells, substantial binding to the surface of U87-MG cells was noted (Figure S1A).

To establish the timeline of entry of the VLPs into U87-MG cells, we monitored the colocalization of Spike protein associated with the VLPs with Rab5, a marker for early endosomes. Endosomal vesicles generated via clathrin-mediated as well as clathrin-independent pathways are known to merge with Rab5-positive early endosomes.[45] For fluorescent labelling of early endosomes, cells were pre-infected by a baculovirus expressing a fusion construct of Rab5a and GFP (CellLight Early Endosomes GFP, Thermo Fisher) for 12 h, which was followed by VLP binding at 37 °C for 5, 15, and 30 min. The fluorescence corresponding to the Spike protein was found to colocalize substantially with Rab5a after 5 min of incubation at 37 °C, indicating the rapid internalization of VLPs into the early endosomal compartments (Figure 3A, top). While the association of the fluorescence corresponding to the Spike protein of VLPs with that of Rab5a remained substantial upon 15 min (Figure 3A, middle) and 30 min (Figure 3A, bottom) of incubation of U87-MG cells with VLPs, there was a marked decrease in colocalization compared to the 5 min time point (~15 and ~40% reduction at the 15 and 30 min time points, respectively; Figure 3B). This decrease in colocalization likely indicates the fusion or maturation of VLP-containing vesicles with late endosomal compartments, although limited coex-

https://doi.org/10.1021/acsinfecdis.2c00217
ACS Infect. Dis. XXXX, XXX, XXX−XXX

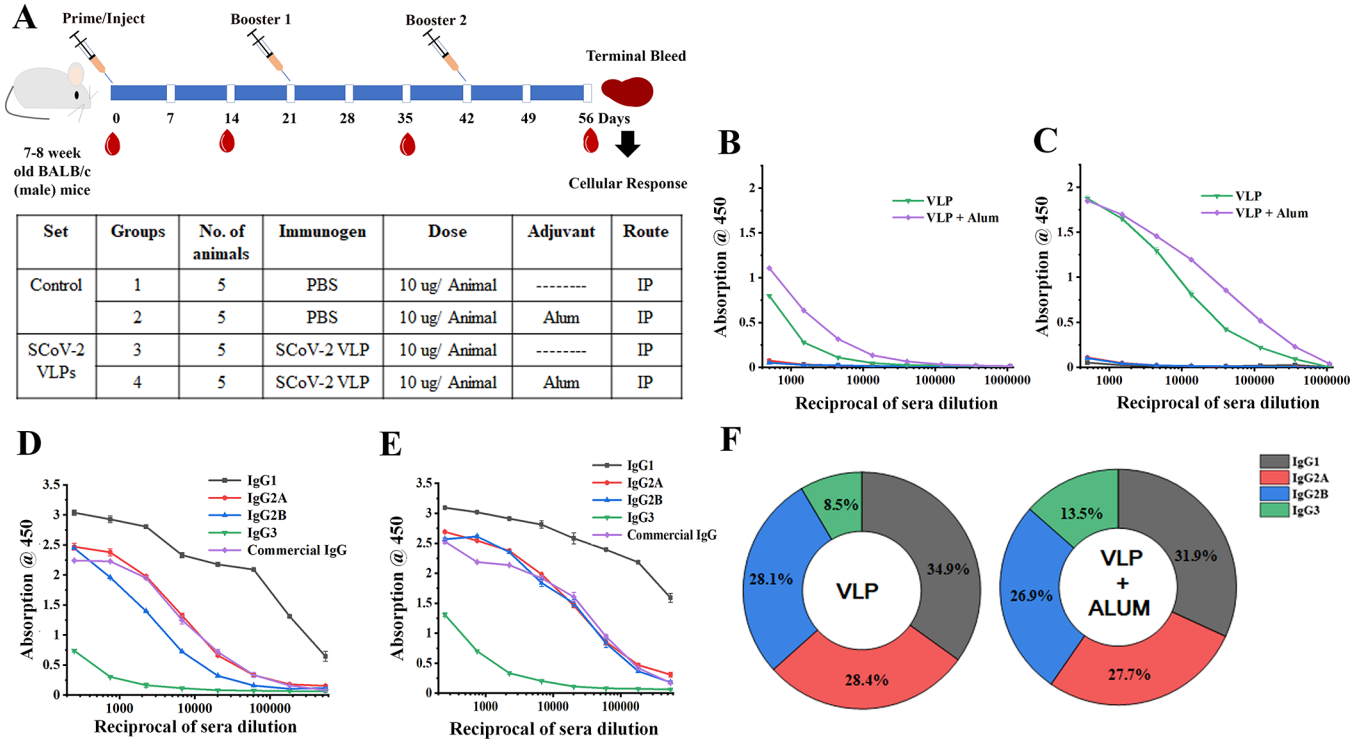

Set	Groups	No. of animals	Immunogen	Dose	Adjuvant	Route
Control	1	5	PBS	10 ug/ Animal	--------	IP
	2	5	PBS	10 ug/ Animal	Alum	IP
SCoV-2 VLPs	3	5	SCoV-2 VLP	10 ug/ Animal	--------	IP
	4	5	SCoV-2 VLP	10 ug/ Animal	Alum	IP

Figure 5. Humoral immune response against SARS-CoV-2 VLPs. (A) Immunization strategy and schedule. (B, C) Antibody response in mice immunized with VLPs in the presence and absence of adjuvants 14 days after the prime and boost injections, respectively. (D, E) IgG subtypes in the immunization groups—VLPs only (D) and VLPs + aluminum hydroxide (E). The corresponding pie charts in (F) represent the contribution of each IgG subclass to the overall immune response in each immunization group. IgG1, IgG2A, IgG2B, and IgG3 responses are represented in gray, red, blue, and green colors respectively.

istence of early and late endosomal markers in the same vesicles have been reported in certain cell types.[45]

Thus, the SARS-CoV-2 VLPs appeared to bind and enter neuronal glioblastoma cells through the endosomal pathway. Interestingly, while HEK293T cells lack both ACE2 and neuropilin, U87-MG cells express a substantial amount of neuropilin on the surface, although there is no notable expression of ACE-2 (Figure S1B). The absence of both ACE-2 and neuropilin likely explains the inability of the VLPs to associate with HEK293T cells. Pre-incubation of U87-MG cells with an anti-neuropilin monoclonal antibody appeared to substantially reduce the binding of SARS-CoV-2 VLPs to the cell surface, indicating that the primary pathway of entry in these cells is through the neuropilin receptor (Figure S1C).

SARS-CoV-2 VLP Entry into U87-MG Cells Is Cholesterol- and Dynamin-Dependent. In order to understand the molecular pathway of VLP entry into glioblastoma cells, the degree of colocalization of the VLP-associated Spike protein with Rab5-positive early endosomes after 15 min of internalization at 37 °C was quantified in the presence of inhibitors. In each case described below, the degree of colocalization was averaged from 10 representative images.

A critical step during both clathrin-mediated and clathrin-independent endocytosis is the scission and release of the nascent endocytic vesicles from the plasma membrane. This step is mediated by dynamin-2, a ubiquitously expressed GTPase, which is also involved in membrane fusion and actin cytoskeleton dynamics.[46] We studied the effect of dynasore, a well-known, effective inhibitor of dynamin-2 on SARS-CoV-2 VLP entry (Figure 4A). Pre-incubation of U87-MG cells with 80 μM of dynasore for 1 h before VLP treatment reduced the colocalization of VLP-associated Spikes with Rab5a-positive early endosomes by ~40% (Figure 4B), indicating the role of dynamin-2 in facilitating the entry of VLPs.

To differentiate the mode of entry of SARS-CoV-2 VLPs, we monitored the localization of the VLPs in early endosomes after an hour-long pre-incubation of cells with 10 μM of chlorpromazine, a widely utilized inhibitor of clathrin-mediated endocytosis. There was a modest decrease in the colocalization of VLP associated Spike and Rab5a in the presence of chlorpromazine (Figure 4A,B). However, pre-incubation of cells with 20 μg/mL of nystatin, a polyene antifungal drug that sequesters cholesterol and inhibits caveolae/lipid raft-mediated entry, reduced colocalization of VLP-associated Spike and Rab5a by approximately 50% (Figure 4A,B). The role of cholesterol-rich regions of the cellular membrane in the early stages of VLP entry was also highlighted by robust inhibition (by ~45%) of VLP trafficking to early endosomes upon pre-incubation of cells with 1 μM filipin for 1 h (Figure 4A,B). Filipin is a chemical reagent that selectively forms complexes with cholesterol in the plasma membrane.[47] A decrease in VLP localization in early endosomes by nystatin and filipin indicates the involvement of cholesterol-rich domains in the early intracellular trafficking of SARS-CoV-2 VLPs in U87-MG cells.

We also checked the effect of pre-incubation of U87-MG cells with the intracellular Ca^{2+} chelator BAPTA-AM on early endosomal localization of the VLPs. Ca^{2+} is one of the most important secondary messengers regulating signaling cascades and the cellular entry, and replication of many pathogenic viruses like coxsackievirus, dengue virus, etc. requires the alteration of cytoplasmic Ca^{2+} homeostasis.[48,49] We noted a modest effect of preincubation of cells with 25 μM BAPTA-

https://doi.org/10.1021/acsinfecdis.2c00217
ACS Infect. Dis. XXXX, XXX, XXX−XXX

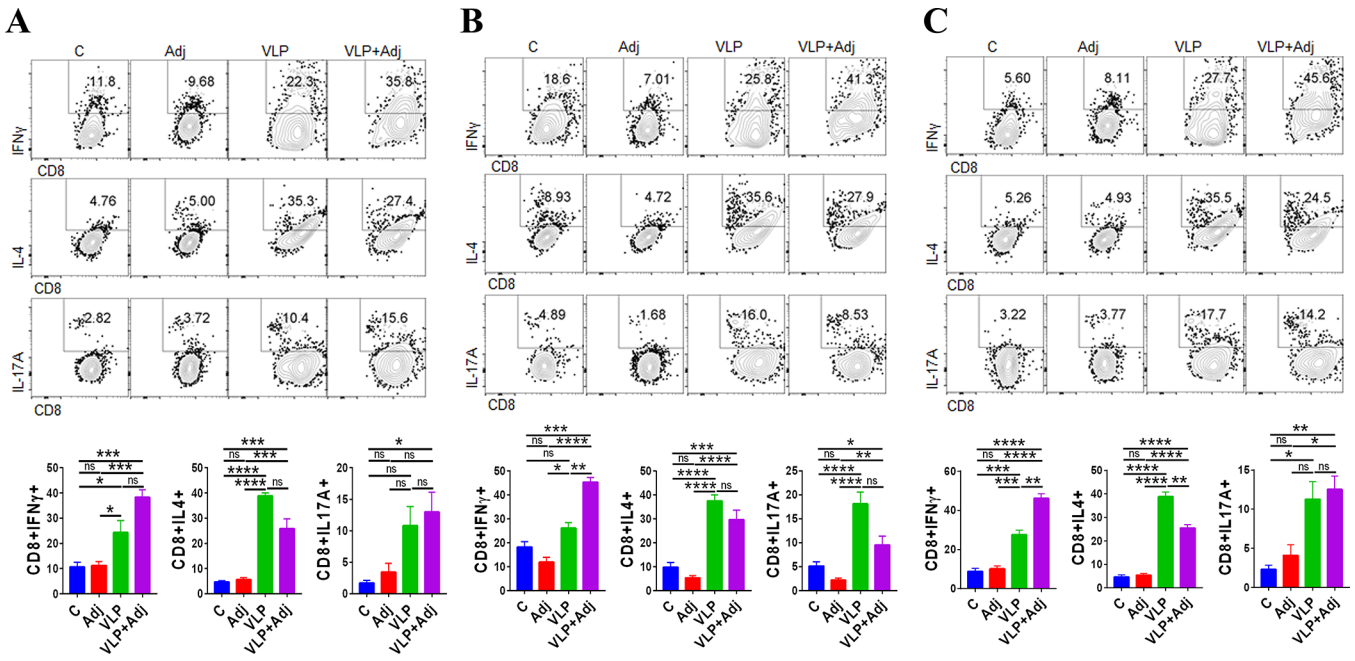

Figure 6. Cellular immune response against SARS-CoV-2 VLPs. (A−C) FACS analysis of cytokine (IFNγ/IL-4/IL-17A) positive cytotoxic T-lymphocytes population upon *in vitro* stimulation of splenocytes isolated from immunized animals with VLPs (A), Spike protein (B), and the nucleocapsid protein from SARS-CoV-2 (C). The top panels show the FACS analysis, while the bottom panels are a quantitative representation of the data. Immunized groups tested here include control (PBS-injected), adjuvant (injected with aluminum hydroxide only), VLP only, and VLP + adjuvant (injected with VLPs in conjunction with aluminum hydroxide). A statistical analysis of the intracellular cytokine staining data was performed by applying a two-way ANOVA for comparison between the groups. The statistically significant values are denoted by $^{*}P < 0.05$, $^{**}P < 0.01$, $^{***}P < 0.001$, and $^{****}P < 0.0001$.

AM on the colocalization of VLP-associated Spike and early endosomal Rab5a (Figure 4A,B).

Thus, while several inhibitors appeared to have a noticeable effect on VLP uptake, pretreatment with dynasore, filipin, and nystatin caused a relatively substantial decrease in VLP colocalization with early endosomes. We, therefore, concluded that the entry of SARS-CoV-2 VLPs in glioblastoma U87-MG cells is primarily mediated through cholesterol and dynamin, while the role of other pathways, including that of clathrin-mediated endocytic process, are relatively modest.

Humoral Immune Response against SARS-CoV-2 VLPs in Mice. The humoral response against SARS-CoV-2 VLPs was studied in BALB/c mice in the absence or presence of an adjuvant aluminum hydroxide.[50] For immunization, five BALB/c male mice in each group were intraperitonially injected with SARS-CoV-2 VLPs only or VLPs with aluminum hydroxide, using a prime/boost type regimen (Figure 5A). The animals were primed on day 0 and boosted with the same formulations (with or without adjuvant) after 21 days and after 42 days following priming. Pre-bleed sera were collected prior to priming, while post-bleed sera were collected at 35 and 56 days (Figure 5A). Control immunizations were carried out with PBS as well as with the adjuvant separately. The humoral response pre- and post-immunization were detected using pooled sera as well as sera from individual animals in a group. The animals were able to tolerate the vaccine and boosting regimen.

Antigen ELISAs with pooled sera collected at 35th day after the initial priming indicated a substantial antibody response against SARS-CoV-2 VLPs (Figure 5B). While the response was the highest in the VLP + aluminum hydroxide group, a significant response was noted for the VLP-only group as well. The antigen responses by the control groups—PBS or adjuvant only, were negligible in comparison. After the second boost at 56 days, a significant increase in the antigen response of the VLP + aluminum hydroxide group was noted (Figure 5C). The sera from the VLP-only group also displayed a robust antigen response, which was almost comparable to that generated by VLPs with adjuvant (Figure 5C). The IgG subclass distribution in the sera post-immunization was analyzed in order to understand the Th1/Th2 polarization of the response to SARS-CoV-2 VLPs. We found that the response was dominated by the IgG1 subclass in the VLPs only group (Figure 5D) as well as in the VLP + adjuvant group (Figure 5E). In all groups, there were substantial IgG2a and IgG2b titers as well as a relatively smaller but significant IgG3 titer (Figure 5D−F). Overall, the distribution of IgG subtypes was similar in the animals immunized with SARS-CoV-2 VLPs only or those immunized with the VLPs in conjunction with alum adjuvant (Figure 5F). A relatively lower IgM response, as compared to the IgG response, was detected as reported elsewhere[51] (Figure S3).

Cellular Immune Response against SARS-CoV-2 VLPs. A robust antigen-specific T cell response is crucial for tackling intracellular pathogen infections including viral infections. The activation of a CD8+ cytotoxic T cell response is required for the recognition and elimination of virus-infected cells. Also, the activation of the CD4+ helper T cells is necessary for stimulation of the innate as well as the adaptive immune response. We investigated the T-cell response in mice immunized with VLPs alone or in conjunction with the adjuvant aluminum hydroxide (Figure 6).

Splenocytes were harvested on the 56th day and restimulated *in vitro* with SARS-CoV-2 VLPs (Figure 6A) or

https://doi.org/10.1021/acsinfecdis.2c00217
ACS Infect. Dis. XXXX, XXX, XXX−XXX

with purified Spike (Figure 6B) and Nucleocapsid (Figure 6C) proteins from SARS-CoV-2. Upon intracellular staining for IFNγ, IL4, and IL17A followed by FACS analysis, we noted a clear expansion in the percentage of cytokine-producing CD8+ cells in the VLP as well as VLP + adjuvant groups compared to control groups. For example, a 2−3-fold increase in the percentage of IFNγ-producing CD8+ T cells in the VLP + adjuvant group compared to the control groups was noted in the antigen-stimulated samples (Figure 6A−C). Particularly, upon stimulation with the N-protein, there was almost an 8-fold increase in the population of IFNγ-producing CD8+ T cells in the VLP + adjuvant group compared to control (Figure 6C). The VLP-only group showed substantial expansion in the population of IFNγ-producing CD8+ T cells in comparison to the control, indicating that the multivalent nature of VLPs may contribute to the activation of cellular immunity in the absence of adjuvants. Also, in all cases of antigen stimulation, a higher percentage of IL4-producing CD8+ T cells was noted in the VLP-only group compared to the VLP + adjuvant group (Figure 6A−C).

An expansion in the percentage of IL-17A-producing CD8+ T cells was noted in the VLP only and VLP + adjuvant group in comparison to control groups. While the percentage of IL-17A positive CD8+ T cells was almost equivalent in both VLP groups upon *in vitro* stimulation with purified VLPs and nucleocapsid protein (Figure 6A,C), there was a substantially increased proportion of IL- 17A-producing CD8+ T cells in the VLP only group upon stimulation with purified Spike protein (Figure 6B). However, the percentage of IL-17A producing CD4+ T cells was significantly higher in the VLP + adjuvant group compared to the VLP-only group upon *in vitro* stimulation with all antigens (Figure S2).

A significant (∼3-fold) increase in IL4-producing CD4+ T cells was noted in the VLP and VLP + adjuvant groups compared to the control in antigen-stimulated cells. Interestingly, when stimulated with N protein, there was a significant expansion of CD4+ T cells secreting IFNγ in the VLP + adjuvant immunized group. However, stimulation with other antigens did not result in a similar elevation in CD4+ T cell IFNγ response (Figure S2). Taken together, this data indicates a substantial cellular immune response against multiple components present in the VLPs, including the Spike and N proteins.

DISCUSSION

The engineering of virus-like particles (VLPs) is a strategy with proven medical and commercial viability. VLPs closely mimic the surface features of native, infectious virions and can be effectively utilized in a variety of applications. Structural similarity with native virions ensures that VLPs will contain analogous immune reactive epitopes, which is desirable in an effective vaccine candidate. VLPs can also be utilized as surrogates for deciphering the molecular interactions and pathways at different stages of virus−host interaction such as receptor interaction, entry, and particle assembly and disassembly. The accessibility of a surrogate system is particularly essential in the case of novel pathogenic viruses with biosafety levels of 3 or 4. In this work, we have generated VLPs of SARS-CoV-2 containing all four major structural protein components of the virus. The antigenicity profile of VLPs clearly indicates the correct positioning of structural proteins Spike (S) and Nucleocapsid (N) in the particles. The morphological features of the VLPs were confirmed by direct visualization using cryoelectron microscopy, which showed the expected brush-like protrusion of spike protein on the surface. The "native-like" features of the VLPs not only imply their suitability as a potential vaccine candidate but also indicate their utility for analyzing the molecular pathway of viral entry in permissive cell lines.

The approved vaccines against SARS-CoV-2, as well as most of the candidates in clinical trials, are based on the immunodominant spike protein of the virus. While this is an excellent strategy, the currently dominating variants like Omicron are cause for concern. The highly transmissible Omicron variant contains a profusion of mutations, including 23 mutations in Spike, some of which overlap with the binding sites of neutralizing antibodies.[52,53] Many countries have implemented a third vaccine (booster) dose to counteract the immune escape properties demonstrated by the Omicron variant. The presence of multiple antigens in a vaccine candidate may ensure efficacy against multiple virus strains, and both M and N proteins have been shown to trigger strong immune responses individually.[36,37] Earlier, the inclusion of the nucleocapsid protein in potential vaccine candidates for β-coronaviruses had indicated the occurrence of lung immunopathology.[54] However, recent studies on inactivated SARS-CoV-2 formulations that contain all structural proteins have moderated such concerns.[10]

A variety of expression systems, including plant, insect, mammalian, and yeast cells, are being utilized for generating native or chimeric VLPs of SARS-CoV-2. Our quadruple antigen particles have been generated by transient transfection of adherent HEK293T cells. While the amount of recombinant protein produced in mammalian cells is significantly lower compared to other expression systems, the post-translational glycosylation pattern—an important consideration for stability as well as immunogenicity of viral glycoproteins—is expected to be the most authentic. HEK293 cells can be adapted to bioreactor-based methods for the large-scale production of proteins.[55] We have established an anion exchange-based method for the purification of VLPs, which is applicable to a large volume of starting material. The elution profile of VLPs from multiple batches of transfected cell culture media clearly shows the propensity of the major VLP fraction to elute consistently at a specific range of NaCl concentration. One distinguishing feature of the VLPs, as compared to the native virions, is particle shape. β-coronaviruses are typically pleomorphic, while the VLPs generated by us appeared to be largely spherical, although there was a significant variation in diameter (80−130 nm). It is possible that the lack of the native genome results in slightly altered morphology in VLPs. Nonetheless, the particles appeared to contain the Spike and Nucleocapsid components in the correct orientation and could trigger appropriate immune responses.

We tested the ability of VLPs, alone or in conjunction with the adjuvant aluminum hydroxide, to elicit effective humoral and cellular immune responses upon injection in mice.

Aluminum salt-based adjuvants have been utilized for vaccination purposes since the early 1930s; however, their mode of functionality remains unclear. The beneficial effect of alum adjuvants is thought to be derived from sequestration of antigens and slow release, by activation of dendritic cells, or by activation of the pro-inflammatory NLRP3 pathway. These adjuvants are thought to encourage Th1- or Th2-type immune responses based on the pathway of administration.[50] However, the antibody response elicited by the VLPs alone was

https://doi.org/10.1021/acsinfecdis.2c00217
ACS Infect. Dis. XXXX, XXX, XXX−XXX

comparable to that generated by VLP + alum post-boosting, which indicated that the multivalent nature of antigen display on VLPs has the potential to trigger an effective immune response in the absence of an adjuvant. VLPs alone, or in conjunction with adjuvant, also stimulated an adequate cellular immune response characterized by clear expansion in the percentage of CD8+ and CD4+ cells producing cytokines like IFNγ, IL4, and IL17A, which are critical for the modulation of both innate and adaptive immune responses. IFNγ is one of the key pro-inflammatory cytokines that are known to be the master regulator of T-cell response to viral pathogenesis and are responsible for the setting up of antiviral states in infected tissues.[56] IL4 regulates Th2 cell-mediated immunity,[57] and IL17 is a unique proinflammatory cytokine released by Th17 cells, innate lymphoid cells (ILCs), and CD8+ T cells, which is thought to link innate and adaptive immune responses in vivo.[58] While the pro-inflammatory action induced by IL17 is thought to be beneficial in the early stages of pathogenesis, significant instances of tissue inflammation and damage have also been attributed to the activation of the IL17-mediated pathways.[58] Interestingly, there was a consistent elevation in the percentage of IL-17A-producing CD4+ T cells in the VLP + adjuvant group compared to the VLP-only group, which was noted upon stimulation with all antigens (N, S, and VLPs) *in vitro*.

The neurotropic potential of human coronaviruses has been reported before,[59] and the presence of SARS-CoV-2 in the cerebrospinal fluid of infected individuals has been confirmed.[60] Although the pathobiology of SARS-CoV-2 is still being established, it is clear that symptoms such as headaches, loss of taste or smell, disturbed consciousness, etc. are signatures of viral invasion in the CNS and its consequent effect on neurological functions.[60] We tested the potential of our VLPs as a replacement for the native virus in cellular interaction studies by analyzing their ability to bind and internalize into neuronal cells. U87-MG cells are epithelial cells derived from a primary human glioblastoma that expresses the neuropilin-1 receptor on the surface, which has recently been identified as an alternative receptor for SARS-CoV-2.[28] It has been shown that the entry of SARS-CoV-2 in the olfactory epithelium, as well as in the neuronal cells, is likely mediated by the neuropilin receptor.[28,29] We found that the VLPs colocalize with Rab5-positive early endosomes after 5 min of cellular association, indicating that the particles can execute the early steps of virus−host interaction. This also indicates that early or late endosomal vesicles could potentially be the sites for Spike-mediated fusion and genome release. Using inhibitors against specific endocytic pathways, we demonstrated that the colocalization of the VLPs with Rab5-positive endosomes is modestly affected by clathrin-mediated endocytosis inhibitors but is reduced significantly by inhibitors of dynamin and cholesterol chelators. This suggests a prominent role for cholesterol-dependent endocytic processes in SARS-CoV-2 entry in neuronal cells. It has been shown earlier that the entry of Spike-pseudotyped lentiviruses in Vero cells or in ACE2-expressing HEK293T cells is mediated by clathrin-mediated endocytosis,[61] although the role of plasma membrane cholesterol in syncytia formation by the virus has been studied.[62] It is possible that the endocytic pathway followed by SARS-CoV-2 is dependent on cell type and the entry in neuronal cells follows a different pathway. A similar difference in viral entry pathways was earlier reported in the case of Japanese encephalitis virus (JEV).[47] The entry pathway of JEV in neuronal cells was reported to be cholesterol- and caveolae-dependent, while that in fibroblasts was primarily through clathrin-mediated endocytosis. The possibility of there being a substantial difference between the cellular interaction of viruses and virus-like particles also exists; however, this is unlikely in the case of VLPs with a similar surface architecture. We also noted that the effect of inhibitors, while substantial, did not entirely abrogate the endocytic localization of VLPs. This indicates the potential involvement of pathways like macropinocytosis, in SARS-CoV-2 VLP entry in U87-MG cells. It has been shown earlier that the entry of CendR peptides through the neuropilin receptor resembles micropinocytosis,[63] which could be an additional pathway exploited by SARS-CoV-2 during entry in neuronal cells.

An understanding of the pathways of viral entry into neuronal cells is crucial for the identification of small molecule or peptide inhibitors of SARS-CoV-2-mediated neurotropism. Our results indicate that VLPs can be effective surrogates for the initial exploration of inhibitory molecules with therapeutic potential.

METHODS

Constructs and Expression. SARS-CoV-2 structural protein sequences were codon-optimized for mammalian cells and synthesized in two pCDNA 3.1+ backbone plasmids. Plasmid 1 contained the sequences for Membrane (M), Envelope (E), Nucleocapsid (N), and the viral Main protease (M^{pro}), while plasmid 2 contained the sequence for spike (S). Adherent HEK293T cells, maintained in DMEM high-glucose media containing 10% FBS and 1% penstrep (GIBCO), were transfected with both plasmids using the transfection reagent jetPRIME (Polyplus) according to the manufacturer's instructions. Transfected cells were incubated for 72 h before media collection for VLP purification.

VLP Purification. The media was first clarified by centrifugation at 9000 rpm at 4 °C for 10 min followed by filtration through a 0.45 μm syringe filter. VLPs were purified from the clarified media by ultracentrifugation through a 30% sucrose cushion at 120,000*g* at 4 °C; the resultant pellet was resuspended in HNE polysorbate buffer (150 mM NaCl, 50 mM HEPES (pH 7.2), 1 mM EDTA, and 0.0005% polysorbate 80), and passed through a 0.22 μm syringe filter to remove debris. For further purification, the particles were loaded on a Hi-Trap Q-XL anion exchange column at 0.5 mL/min and 30 min with AKTA pure 25 FPLC (GE) and eluted using a gradient of 50 mM HEPES (pH 7.2), 1 mM DTT, and 1 M NaCl. Peak fractions were collected, dialyzed in HNE polysorbate buffer, and concentrated using an Amicon filter with a 100 kDa cutoff (Merck) and stored at 4 °C. Total protein concentration was estimated using a Bradford assay.

Purification of SARS-CoV-2 Spike and Nucleocapsid Proteins. Recombinant SARS CoV-2 spike and N proteins were expressed and purified as described in our previous work.[42,64] Briefly, the codon-optimized sequence of Spike-His was expressed in Expi 293F cells, and the culture supernatant harvested 7 days post-transfection was purified by Ni-NTA affinity chromatography, followed by dialysis in phosphate-buffered saline (pH 7.4). The SARS-CoV-2 N protein was expressed in the bacterial expression system and purified by Ni-NTA affinity chromatography. Post purification, the protein was dialyzed in 50 mM Tris (pH 8.0), 150 mM NaCl, and 2 mM EDTA.

https://doi.org/10.1021/acsinfecdis.2c00217
ACS Infect. Dis. XXXX, XXX, XXX−XXX

Western Blotting. VLP samples separated on 10% SDS-PAGE were transferred onto PVDF membranes and blocked with 5% skim milk in TBS-T for 2 h at room temperature. This was followed by three washes with TBS-T and incubation with primary antibodies against Spike (Invitrogen PA1-41513), Nucleocapsid (R&D Systems, MAB10474), and Membrane proteins (Arigo Biolaboratories ARG54884), overnight at 4 °C. After washes, HRP-conjugated anti-rabbit (Santa Cruz Biotechnology sc-2004) and anti-mouse (Santa Cruz Biotechnology, sc-2005) secondary antibodies were added as appropriate. The blots were developed with ECL plus reagent (Thermo Fisher) and imaged using a Typhoon FLA 900 (GE).

Dynamic Light Scattering. One microliter of the sample was added to 49 μL of DPBS in a quartz cuvette and analyzed in a Wyatt DAWN8+ MALS with the software ASTRA. A regularized hydrodynamic radius of particle population was obtained after normalization.

Electron Microscopy. For negative-stain EM, 5 μL of the sample was applied to glow-discharged carbon-coated copper grids for 1 min, followed by removal of the excess sample using Whatman filter paper (1001125) and staining with 2% uranyl acetate. After washes, the grid was air-dried and visualized in an FEI Tecnai F20 TEM (Thermo Fisher) operating at 200 kV. For cryoelectron microscopy, 5 μL of the sample was applied to a glow-discharged gold coated quantifoil grid for 1 min, followed by quick-freezing of the grid in a Vitrobot Mark IV (Thermo Fisher) at optimized conditions of temperature and humidity and visualization in an FEI Tecnai F20 TEM (Thermo Fisher) operating at 200 kV, at magnifications of 29−50k× with a defocus range of −3 to −5 μm.

hACE2 Binding Analysis. The binding specificity of SARS CoV-2 VLP to the ACE2 receptor (hACE2-Fc ELISA) was estimated through ELISA. Briefly, Maxisorp plates (Nunc) were coated with 100 μL of VLP (2 μg/mL concentration) in 1× carbonate/bicarbonate and processed further as described.[65,66] hACE2-Fc protein, at a starting concentration of 10 mg/mL, was serially diluted to 1:3, incubated, and processed further as described.[65] HRP-conjugated anti-human antibody (1:10,000 dilution, Jackson Immuno Research, USA) was utilized as a secondary antibody, and the signals were measured at OD_{450} using an ELISA plate reader.

Animal Immunization. All animal immunization studies were carried out in the small animal facility (SAF) of the Translational Health Science and Technology Institute (THSTI, Faridabad, Haryana) as per the approved Institutional Animal Ethics Protocol. Seven to eight week old BALB/c (male) mice (five animals per group) were immunized with either 10 μg of SARS-CoV-2 VLPs alone or in conjunction with aluminum hydroxide adjuvant (1:1 ratio). Control groups were immunized with PBS only or with adjuvant only. The prime/boost protocol described in Figure 5A was followed. For each immunization, mice were bled 14 days later, and the sera were stored at −80 °C until further use.

Ethics Statement. The animal immunization studies were performed at the Small Animal Facility (SAF) of Translational Health Science and Technology Institute, NCR Biotech Science Cluster, Faridabad, India, with registration number: 1685/GO/ReBi/S/2013/CPCSEA. The studies were performed in accordance with the Institutional Animal Ethics Committee (IAEC) approval of THSTI (approval number IAEC/THSTI/122) for the project titled "Evaluating the immunogenicity of a virus-like particle-based vaccine candidate against SARS CoV-2". All protocols for the care and use of laboratory animals were strictly followed.

ELISA Assays. Indirect ELISA assays were performed to characterize the binding of SARS-CoV-2 VLPs against anti-SARS-CoV-2 sera and commercial antibodies as described previously.[65,66] Briefly, 2 μg/mL purified SARS-CoV-2 VLPs in 1× carbonate buffer (pH 9.6) were used to coat 96-well MaxiSorp plates (Nunc) and incubated overnight at 4 °C. After incubation, blocking was carried out with 5% skimmed milk for 1 h at 37 °C. Anti-SARS-CoV-2 RBD-, Spike-, or N directed-polyclonal sera (1:100) were serially diluted in 1% skimmed milk and added at 37 °C for 1 h. In addition, commercial monoclonal and polyclonal primary antibodies against the Spike (GTX632604 and GTX135356, Genetex) and N proteins (GTX632269 and GTX135357, GeneTex) were also used, at a concentration of 10 μg/mL, to characterize the binding specificity of SARS-CoV-2 VLPs. The plates were washed three times with 1× PBST, followed by incubation for 1 h at 37 °C with HRP-labeled secondary antibodies (anti-mouse or anti-rabbit, Sigma) at 1:2000 dilution and addition of the chromogenic substrate tetramethylbenzidine (TMB) in the dark for 10 min at room temperature. The signal was measured at OD_{450} using an ELISA plate reader.

ELISA assays were performed similarly with pooled sera from mice injected with VLPs only or VLPs + adjuvant and collected 14 days after the prime and boost injections. Ninety-six-well MaxiSorp plates (Nunc) were coated with SARS-CoV-2 VLPs at a concentration of 2 μg/mL. The sera were serially diluted to 1:3, with a starting dilution of 1:250 in 1% skimmed milk, and were added to the coated plates for 1 h at 37° C. The plates were washed and treated with HRP-labeled mouse secondary antibody at a dilution of 1:2000. The signal obtained from treatment with TMB substrate was measured at OD_{450} using an ELISA plate reader.

The IgM response was also quantified for immunization groups of VLPs only and VLP + adjuvant. ELISA was performed with pre-bleed, prime, and boost injection sera on SARS-CoV-2 VLP coated plates as described above.

IgG Subtyping. Purified SARS-CoV-2 VLPs, at a concentration of 2 μg/mL in 1× carbonate buffer (pH 9.6), was used to coat 96-well MaxiSorp plates (Nunc) at 4 °C. After overnight incubation, the plate was blocked with 5% skimmed milk for 1 h at 37 °C. Pooled sera from mice injected with VLPs only or VLPs + adjuvant were serially diluted 1:3 times, with a starting dilution of 1:250 in 1% skimmed milk, and were added to the coated plates for 1 h at 37 °C. The plates were washed thrice with 1× PBST, followed by incubation for 1 h at 37 °C with HRP-labeled secondary antibodies against IgG1, IgG2a, IgG2b, IgG3, and commercial IgG (anti-mouse, Sigma) at 1:2000 dilution. This was followed by addition of the chromogenic substrate tetramethylbenzidine (TMB) incubation in the dark for 10 min at room temperature. The signal was measured at OD_{450} using an ELISA plate reader.

In Vitro Stimulation of Splenocytes and Intracellular Cytokine Staining. Splenocytes collected from immunized animals were stimulated in 96-well plates with purified VLPs or recombinant protein antigens Spike, RBD, or the N protein at 37 °C for 72 h in a 5% CO_2 incubator. Post-stimulation, cells were pelleted and stained for surface CD4-PerCp and CD8-FITC in the dark at 20 min (RT). Following permeabilization and fixation with BD Cytofix, cells were stained for cytokines IFNγ, IL-17A, and IL-4 in the dark for 20 min (RT). After

https://doi.org/10.1021/acsinfecdis.2c00217
ACS Infect. Dis. XXXX, XXX, XXX−XXX

washing, FACS data were acquired on a BD FACS Canto II machine, and the data was analyzed using FlowJo (Tree Star).

Confocal Laser Scanning Microscopy. U87-MG or HEK293T cells (3×10^4) were seeded on cleaned, 0.01% poly-L-lysine-treated 18 mm glass coverslips (Sigma) and incubated overnight. For labelling endosomal compartments, cells were incubated with CellLight early endosomes−GFP (Life Technologies) for ≥16 h according to the manufacturer's instructions. SARS-CoV-2 VLPs were added to cells for 1 h at 4 °C for binding analysis or at 37 °C for monitoring internalization. After three washes with DPBS, cells were fixed in 4% paraformaldehyde for 15 min, permeabilized with 0.2% Triton X-100, and blocked with 1% BSA. For visualization of VLPs, a rabbit polyclonal SARS-CoV-2 Spike primary antibody (Invitrogen PA1-41513) was utilized in conjunction with Alexa Fluor 555-labeled goat anti-rabbit antibody (Invitrogen A-21428). For detection of the neuropilin-1 receptor, a rabbit neuropilin-1 primary antibody (Abcam ab81321) and an Alexa Fluor 555-labeled goat anti-rabbit antibody (Invitrogen A-21428) were used. Mouse antisera against hACE-2 and an Alexa Fluor 594-labeled goat anti-mouse antibody (A-11032) were used to detect the hACE-2 receptor. The neuropilin receptor was blocked with a rabbit neuropilin-1 primary antibody (Abcam ab81321), followed by treatment of the cells with SARS-CoV-2 VLPs. For detection of VLPs, a mouse SARS-CoV-2 Spike monoclonal antibody (GTX632604) in conjunction with an Alexa Fluor 594 goat anti-mouse antibody (A-11032) was utilized.

For the inhibition of VLP uptake, U87-MG cells were seeded and grown at 37 °C for 24 h and treated with inhibitors dynasore (D7693-Sigma) (80 μM, 1 h), chlorpromazine (C8138-Sigma) (10 μM, 1 h), nystatin (N6261-Sigma) (20 μg/ml, 30 min), ammonium chloride (A9434-Sigma) (50 mM, 1 h), BAPTA (A1076-Sigma) (25 μM, 30 min), and filipin (F9765-Sigma) (1 μM, 1 h). The cells were treated with SCoV2-VLPs for 5 min at 37 °C, washed thrice with 1× PBS, fixed with 4% paraformaldehyde, permeabilized with 0.1% TritonX-100, and immunostained with anti-spike primary antibody (Invitrogen PA1-41513) in conjunction with Alexa Fluor 555-labeled goat anti-rabbit IgG secondary antibody (Invitrogen A-21428). Nuclei were labeled with 300 nM DAPI (Invitrogen D1306) for 10 min. After washing in DPBS, cells were mounted using Prolong Glass Antifade Mountant (Invitrogen P36982), dried, and sealed. Images were collected in a confocal microscope (Leica DMi8) at a magnification of 63×, oil immersion. For each dataset, the colocalization efficiency as per Pearson's coefficient was calculated from 10 confocal microscopy images collected from multiple fields of view in multiple slides.

■ ASSOCIATED CONTENT

Supporting Information

The Supporting Information is available free of charge at https://pubs.acs.org/doi/10.1021/acsinfecdis.2c00217.

Association of VLPs with HEK293T and U87-MG cells at 4 °C; occurrence of neuropilin-1 and hACE-2 receptors on U87-MG cells; effect of pre-blocking of neuropilin receptor with an anti-neuropilin antibody followed by treatment with VLP versus VLP treatment only; FACS analysis of cytokine (IFNγ/IL-4/IL-17A)-positive helper T-lymphocyte (CD4+) population upon *in vitro* stimulation of splenocytes isolated from immunized animals with VLPs, spike protein, and nucleocapsid protein from SARS-CoV-2; IgM immune response in treatments of VLP only and VLP with aluminum hydroxide (PDF)

■ AUTHOR INFORMATION

Corresponding Author

Manidipa Banerjee − *Kusuma School of Biological Sciences, Indian Institute of Technology Delhi, New Delhi 110016, India;* orcid.org/0000-0001-6202-5965; Email: mbanerjee@bioschool.iitd.ac.in

Authors

Chandra Shekhar Kumar − *Kusuma School of Biological Sciences, Indian Institute of Technology Delhi, New Delhi 110016, India*

Balwant Singh − *Translational Health Science and Technology Institute (THSTI), Faridabad, Haryana 121001, India*

Zaigham Abbas Rizvi − *Translational Health Science and Technology Institute (THSTI), Faridabad, Haryana 121001, India; Immunobiology/Immunology Core Laboratory, Translational Health Science and Technology Institute (THSTI), Faridabad, Haryana 121001, India*

Hilal Ahmad Parray − *Translational Health Science and Technology Institute (THSTI), Faridabad, Haryana 121001, India*

Jitender Kumar Verma − *Kusuma School of Biological Sciences, Indian Institute of Technology Delhi, New Delhi 110016, India*

Sukanya Ghosh − *Kusuma School of Biological Sciences, Indian Institute of Technology Delhi, New Delhi 110016, India*

Amitabha Mukhopadhyay − *Kusuma School of Biological Sciences, Indian Institute of Technology Delhi, New Delhi 110016, India*

Amit Awasthi − *Translational Health Science and Technology Institute (THSTI), Faridabad, Haryana 121001, India; Immunobiology/Immunology Core Laboratory, Translational Health Science and Technology Institute (THSTI), Faridabad, Haryana 121001, India*

Tripti Shrivastava − *Translational Health Science and Technology Institute (THSTI), Faridabad, Haryana 121001, India*

Complete contact information is available at: https://pubs.acs.org/10.1021/acsinfecdis.2c00217

Author Contributions

[‖]Present address: The Wistar Institute, 3601 Spruce Street, Philadelphia, PA 19104, USA

Author Contributions

C.S.K., B.S., Z.A.R., J.K.V., and S.G. conducted the experiments. C.S.K., Z.A.R., T.S., A.A., A.M., and M.B. designed the experiments. H.A.P. performed the animal immunization, and Z.A.R. and A.A. performed the T cell assay. C.S.K., B.S., Z.A.R., A.M., T.S., A.A., and M.B. analyzed the data. C.S.K., T.S., and M.B. wrote the manuscript.

Notes

The authors declare no competing financial interest.

https://doi.org/10.1021/acsinfecdis.2c00217
ACS Infect. Dis. XXXX, XXX, XXX−XXX

■ ACKNOWLEDGMENTS

The authors acknowledge the Central Research Facility of IIT-Delhi and Mr. Akshey Kaushal for technical help with cryoelectron microscopy data collection. We would like to thank the THSTI SAF (Small Animal Facility) staff for providing animals for the studies. We also acknowledge the THSTI Immunology Core Facility (ICF) for supporting our immunization and immunogenicity studies. pcDNA3-sACE2 (wt)−Fc(IgG1) was a kind gift from Dr. Erik Procko (Addgene plasmid no. 145163). The work in this manuscript is protected by Indian provisional patent application no. 202111005428.

■ REFERENCES

(1) Andersen, K. G.; Rambaut, A.; Lipkin, W. I.; Holmes, E. C.; Garry, R. F. The proximal origin of SARS-CoV-2. *Nat. Med.* **2020**, *26*, 450−452.

(2) Pang, J.; Wang, M. X.; Ang, I. Y. H.; Tan, S. H. X.; Lewis, R. F.; Chen, J. I.; Gutierrez, R. A.; Gwee, S. X. W.; Chua, P. E. Y.; Yang, Q.; Ng, X. Y.; Yap, R. K.; Tan, H. Y.; Teo, Y. Y.; Tan, C. C.; Cook, A. R.; Yap, J. C.; Hsu, L. Y. Potential Rapid Diagnostics, Vaccine and Therapeutics for 2019 Novel Coronavirus (2019-nCoV): A Systematic Review. *J. Clin. Med.* **2020**, *9*, 623.

(3) Shih, H. I.; Wu, C. J.; Tu, Y. F.; Chi, C. Y. Fighting COVID-19: A quick review of diagnoses, therapies, and vaccines. *Biomed. J.* **2020**, *43*, 341−354.

(4) Beigel, J. H.; Tomashek, K. M.; Dodd, L. E.; Mehta, A. K.; Zingman, B. S.; Kalil, A. C.; Hohmann, E.; Chu, H. Y.; Luetkemeyer, A.; Kline, S.; Lopez de Castilla, D.; Finberg, R. W.; Dierberg, K.; Tapson, V.; Hsieh, L.; Patterson, T. F.; Paredes, R.; Sweeney, D. A.; Short, W. R.; Touloumi, G.; Lye, D. C.; Ohmagari, N.; Oh, M. D.; Ruiz-Palacios, G. M.; Benfield, T.; Fatkenheuer, G.; Kortepeter, M. G.; Atmar, R. L.; Creech, C. B.; Lundgren, J.; Babiker, A. G.; Pett, S.; Neaton, J. D.; Burgess, T. H.; Bonnett, T.; Green, M.; Makowski, M.; Osinusi, A.; Nayak, S.; Lane, H. C.; Members, A.-S. G. Remdesivir for the Treatment of Covid-19 - Final Report. *N. Engl. J. Med.* **2020**, *383*, 1813−1826.

(5) Grein, J.; Ohmagari, N.; Shin, D.; Diaz, G.; Asperges, E.; Castagna, A.; Feldt, T.; Green, G.; Green, M. L.; Lescure, F. X.; Nicastri, E.; Oda, R.; Yo, K.; Quiros-Roldan, E.; Studemeister, A.; Redinski, J.; Ahmed, S.; Bernett, J.; Chelliah, D.; Chen, D.; Chihara, S.; Cohen, S. H.; Cunningham, J.; D'Arminio Monforte, A.; Ismail, S.; Kato, H.; Lapadula, G.; L'Her, E.; Maeno, T.; Majumder, S.; Massari, M.; Mora-Rillo, M.; Mutoh, Y.; Nguyen, D.; Verweij, E.; Zoufaly, A.; Osinusi, A. O.; DeZure, A.; Zhao, Y.; Zhong, L.; Chokkalingam, A.; Elboudwarej, E.; Telep, L.; Timbs, L.; Henne, I.; Sellers, S.; Cao, H.; Tan, S. K.; Winterbourne, L.; Desai, P.; Mera, R.; Gaggar, A.; Myers, R. P.; Brainard, D. M.; Childs, R.; Flanigan, T. Compassionate Use of Remdesivir for Patients with Severe Covid-19. *N. Engl. J. Med.* **2020**, *382*, 2327−2336.

(6) Wang, Y.; Zhang, D.; Du, G.; Du, R.; Zhao, J.; Jin, Y.; Fu, S.; Gao, L.; Cheng, Z.; Lu, Q.; Hu, Y.; Luo, G.; Wang, K.; Lu, Y.; Li, H.; Wang, S.; Ruan, S.; Yang, C.; Mei, C.; Wang, Y.; Ding, D.; Wu, F.; Tang, X.; Ye, X.; Ye, Y.; Liu, B.; Yang, J.; Yin, W.; Wang, A.; Fan, G.; Zhou, F.; Liu, Z.; Gu, X.; Xu, J.; Shang, L.; Zhang, Y.; Cao, L.; Guo, T.; Wan, Y.; Qin, H.; Jiang, Y.; Jaki, T.; Hayden, F. G.; Horby, P. W.; Cao, B.; Wang, C. Remdesivir in adults with severe COVID-19: a randomised, double-blind, placebo-controlled, multicentre trial. *Lancet* **2020**, *395*, 1569−1578.

(7) Wang, X.; Peng, W.; Ren, J.; Hu, Z.; Xu, J.; Lou, Z.; Li, X.; Yin, W.; Shen, X.; Porta, C.; Walter, T. S.; Evans, G.; Axford, D.; Owen, R.; Rowlands, D. J.; Wang, J.; Stuart, D. I.; Fry, E. E.; Rao, Z. A sensor-adaptor mechanism for enterovirus uncoating from structures of EV71. *Nat. Struct. Mol. Biol.* **2012**, *19*, 424−429.

(8) Wang, H.; Zhang, Y.; Huang, B.; Deng, W.; Quan, Y.; Wang, W.; Xu, W.; Zhao, Y.; Li, N.; Zhang, J.; Liang, H.; Bao, L.; Xu, Y.; Ding, L.; Zhou, W.; Gao, H.; Liu, J.; Niu, P.; Zhao, L.; Zhen, W.; Fu, H.; Yu, S.; Zhang, Z.; Xu, G.; Li, C.; Lou, Z.; Xu, M.; Qin, C.; Wu, G.; Gao, G. F.; Tan, W.; Yang, X. Development of an Inactivated Vaccine Candidate, BBIBP-CorV, with Potent Protection against SARS-CoV-2. *Cell* **2020**, *182*, 713−721.e9.

(9) Jackson, L. A.; Anderson, E. J.; Rouphael, N. G.; Roberts, P. C.; Makhene, M.; Coler, R. N.; McCullough, M. P.; Chappell, J. D.; Denison, M. R.; Stevens, L. J.; Pruijssers, A. J.; McDermott, A.; Flach, B.; Doria-Rose, N. A.; Corbett, K. S.; Morabito, K. M.; O'Dell, S.; Schmidt, S. D.; Swanson, P. A., 2nd; Padilla, M.; Mascola, J. R.; Neuzil, K. M.; Bennett, H.; Sun, W.; Peters, E.; Makowski, M.; Albert, J.; Cross, K.; Buchanan, W.; Pikaart-Tautges, R.; Ledgerwood, J. E.; Graham, B. S.; Beigel, J. H. m. R. N. A. S. G. An mRNA Vaccine against SARS-CoV-2 - Preliminary Report. *N. Engl. J. Med.* **2020**, *383*, 1920−1931.

(10) Gao, Q.; Bao, L.; Mao, H.; Wang, L.; Xu, K.; Yang, M.; Li, Y.; Zhu, L.; Wang, N.; Lv, Z.; Gao, H.; Ge, X.; Kan, B.; Hu, Y.; Liu, J.; Cai, F.; Jiang, D.; Yin, Y.; Qin, C.; Li, J.; Gong, X.; Lou, X.; Shi, W.; Wu, D.; Zhang, H.; Zhu, L.; Deng, W.; Li, Y.; Lu, J.; Li, C.; Wang, X.; Yin, W.; Zhang, Y.; Qin, C. Development of an inactivated vaccine candidate for SARS-CoV-2. *Science* **2020**, *369*, 77−81.

(11) Spruth, M.; Kistner, O.; Savidis-Dacho, H.; Hitter, E.; Crowe, B.; Gerencer, M.; Bruhl, P.; Grillberger, L.; Reiter, M.; Tauer, C.; Mundt, W.; Barrett, P. N. A double-inactivated whole virus candidate SARS coronavirus vaccine stimulates neutralising and protective antibody responses. *Vaccine* **2006**, *24*, 652−661.

(12) Garcea, R. L.; Gissmann, L. Virus-like particles as vaccines and vessels for the delivery of small molecules. *Curr. Opin. Biotechnol.* **2004**, *15*, 513−517.

(13) Wang, J. W.; Roden, R. B. Virus-like particles for the prevention of human papillomavirus-associated malignancies. *Expert Rev. Vaccines* **2013**, *12*, 129−141.

(14) Mortola, E.; Roy, P. Efficient assembly and release of SARS coronavirus-like particles by a heterologous expression system. *FEBS Lett.* **2004**, *576*, 174−178.

(15) Jiang, S.; He, Y.; Liu, S. SARS vaccine development. *Emerging Infect. Dis.* **2005**, *11*, 1016−1020.

(16) Liu, Y. V.; Massare, M. J.; Barnard, D. L.; Kort, T.; Nathan, M.; Wang, L.; Smith, G. Chimeric severe acute respiratory syndrome coronavirus (SARS-CoV) S glycoprotein and influenza matrix 1 efficiently form virus-like particles (VLPs) that protect mice against challenge with SARS-CoV. *Vaccine* **2011**, *29*, 6606−6613.

(17) Kato, T.; Takami, Y.; Kumar Deo, V.; Park, E. Y. Preparation of virus-like particle mimetic nanovesicles displaying the S protein of Middle East respiratory syndrome coronavirus using insect cells. *J. Biotechnol.* **2019**, *306*, 177−184.

(18) Li, E.; Yan, F.; Huang, P.; Chi, H.; Xu, S.; Li, G.; Liu, C.; Feng, N.; Wang, H.; Zhao, Y.; Yang, S.; Xia, X. Characterization of the Immune Response of MERS-CoV Vaccine Candidates Derived from Two Different Vectors in Mice. *Viruses* **2020**, *12*, 125.

(19) Wang, C.; Zheng, X.; Gai, W.; Wong, G.; Wang, H.; Jin, H.; Feng, N.; Zhao, Y.; Zhang, W.; Li, N.; Zhao, G.; Li, J.; Yan, J.; Gao, Y.; Hu, G.; Yang, S.; Xia, X. Novel chimeric virus-like particles vaccine displaying MERS-CoV receptor-binding domain induce specific humoral and cellular immune response in mice. *Antiviral Res.* **2017**, *140*, 55−61.

(20) Naskalska, A.; Dabrowska, A.; Nowak, P.; Szczepanski, A.; Jasik, K.; Milewska, A.; Ochman, M.; Zeglen, S.; Rajfur, Z.; Pyrc, K. Novel coronavirus-like particles targeting cells lining the respiratory tract. *PLoS One* **2018**, *13*, No. e0203489.

(21) Plescia, C. B.; David, E. A.; Patra, D.; Sengupta, R.; Amiar, S.; Su, Y.; Stahelin, R. V. SARS-CoV-2 viral budding and entry can be modeled using BSL-2 level virus-like particles. *J. Biol. Chem.* **2021**, *296*, 100103.

(22) Neuman, B. W.; Kiss, G.; Kunding, A. H.; Bhella, D.; Baksh, M. F.; Connelly, S.; Droese, B.; Klaus, J. P.; Makino, S.; Sawicki, S. G.; Siddell, S. G.; Stamou, D. G.; Wilson, I. A.; Kuhn, P.; Buchmeier, M. J. A structural analysis of M protein in coronavirus assembly and morphology. *J. Struct. Biol.* **2011**, *174*, 11−22.

https://doi.org/10.1021/acsinfecdis.2c00217
ACS Infect. Dis. XXXX, XXX, XXX−XXX

(23) Ruch, T. R.; Machamer, C. E. The coronavirus E protein: assembly and beyond. *Viruses* **2012**, *4*, 363−382.
(24) Bosch, B. J.; van der Zee, R.; de Haan, C. A.; Rottier, P. J. The coronavirus spike protein is a class I virus fusion protein: structural and functional characterization of the fusion core complex. *J. Virol.* **2003**, *77*, 8801−8811.
(25) Hulswit, R. J.; de Haan, C. A.; Bosch, B. J. Coronavirus Spike Protein and Tropism Changes. *Adv. Virus Res.* **2016**, *96*, 29−57.
(26) Lan, J.; Ge, J.; Yu, J.; Shan, S.; Zhou, H.; Fan, S.; Zhang, Q.; Shi, X.; Wang, Q.; Zhang, L.; Wang, X. Structure of the SARS-CoV-2 spike receptor-binding domain bound to the ACE2 receptor. *Nature* **2020**, *581*, 215−220.
(27) Wang, Q.; Zhang, Y.; Wu, L.; Niu, S.; Song, C.; Zhang, Z.; Lu, G.; Qiao, C.; Hu, Y.; Yuen, K. Y.; Wang, Q.; Zhou, H.; Yan, J.; Qi, J. Structural and Functional Basis of SARS-CoV-2 Entry by Using Human ACE2. *Cell* **2020**, *181*, 894−904.e9.
(28) Cantuti-Castelvetri, L.; Ojha, R.; Pedro, L. D.; Djannatian, M.; Franz, J.; Kuivanen, S.; van der Meer, F.; Kallio, K.; Kaya, T.; Anastasina, M.; Smura, T.; Levanov, L.; Szirovicza, L.; Tobi, A.; Kallio-Kokko, H.; Osterlund, P.; Joensuu, M.; Meunier, F. A.; Butcher, S. J.; Winkler, M. S.; Mollenhauer, B.; Helenius, A.; Gokce, O.; Teesalu, T.; Hepojoki, J.; Vapalahti, O.; Stadelmann, C.; Balistreri, G.; Simons, M. Neuropilin-1 facilitates SARS-CoV-2 cell entry and infectivity. *Science* **2020**, *370*, 856−860.
(29) Daly, J. L.; Simonetti, B.; Klein, K.; Chen, K. E.; Williamson, M. K.; Anton-Plagaro, C.; Shoemark, D. K.; Simon-Gracia, L.; Bauer, M.; Hollandi, R.; Greber, U. F.; Horvath, P.; Sessions, R. B.; Helenius, A.; Hiscox, J. A.; Teesalu, T.; Matthews, D. A.; Davidson, A. D.; Collins, B. M.; Cullen, P. J.; Yamauchi, Y. Neuropilin-1 is a host factor for SARS-CoV-2 infection. *Science* **2020**, *370*, 861−865.
(30) McBride, R.; van Zyl, M.; Fielding, B. C. The coronavirus nucleocapsid is a multifunctional protein. *Viruses* **2014**, *6*, 2991−3018.
(31) Kang, S.; Yang, M.; Hong, Z.; Zhang, L.; Huang, Z.; Chen, X.; He, S.; Zhou, Z.; Zhou, Z.; Chen, Q.; Yan, Y.; Zhang, C.; Shan, H.; Chen, S. Crystal structure of SARS-CoV-2 nucleocapsid protein RNA binding domain reveals potential unique drug targeting sites. *Acta Pharm. Sin. B* **2020**, *10*, 1228−1238.
(32) Siu, Y. L.; Teoh, K. T.; Lo, J.; Chan, C. M.; Kien, F.; Escriou, N.; Tsao, S. W.; Nicholls, J. M.; Altmeyer, R.; Peiris, J. S.; Bruzzone, R.; Nal, B. The M, E, and N structural proteins of the severe acute respiratory syndrome coronavirus are required for efficient assembly, trafficking, and release of virus-like particles. *J. Virol.* **2008**, *82*, 11318−11330.
(33) Janice, O. H. L.; Ken-En Gan, S.; Bertoletti, A.; Tan, Y. J. Understanding the T cell immune response in SARS coronavirus infection. *Emerging Microbes Infect.* **2012**, *1*, No. e23.
(34) Li, C. K.; Wu, H.; Yan, H.; Ma, S.; Wang, L.; Zhang, M.; Tang, X.; Temperton, N. J.; Weiss, R. A.; Brenchley, J. M.; Douek, D. C.; Mongkolsapaya, J.; Tran, B. H.; Lin, C. L.; Screaton, G. R.; Hou, J. L.; McMichael, A. J.; Xu, X. N. T cell responses to whole SARS coronavirus in humans. *J. Immunol.* **2008**, *181*, 5490−5500.
(35) Le Bert, N.; Tan, A. T.; Kunasegaran, K.; Tham, C. Y. L.; Hafezi, M.; Chia, A.; Chng, M. H. Y.; Lin, M.; Tan, N.; Linster, M.; Chia, W. N.; Chen, M. I.; Wang, L. F.; Ooi, E. E.; Kalimuddin, S.; Tambyah, P. A.; Low, J. G.; Tan, Y. J.; Bertoletti, A. SARS-CoV-2-specific T cell immunity in cases of COVID-19 and SARS, and uninfected controls. *Nature* **2020**, *584*, 457−462.
(36) Liu, J.; Sun, Y.; Qi, J.; Chu, F.; Wu, H.; Gao, F.; Li, T.; Yan, J.; Gao, G. F. The membrane protein of severe acute respiratory syndrome coronavirus acts as a dominant immunogen revealed by a clustering region of novel functionally and structurally defined cytotoxic T-lymphocyte epitopes. *J. Infect. Dis.* **2010**, *202*, 1171−1180.
(37) Ng, O. W.; Chia, A.; Tan, A. T.; Jadi, R. S.; Leong, H. N.; Bertoletti, A.; Tan, Y. J. Memory T cell responses targeting the SARS coronavirus persist up to 11 years post-infection. *Vaccine* **2016**, *34*, 2008−2014.
(38) Huang, Y.; Yang, C.; Xu, X. F.; Xu, W.; Liu, S. W. Structural and functional properties of SARS-CoV-2 spike protein: potential antivirus drug development for COVID-19. *Acta Pharmacol. Sin.* **2020**, *41*, 1141−1149.
(39) Walls, A. C.; Park, Y. J.; Tortorici, M. A.; Wall, A.; McGuire, A. T.; Veesler, D. Structure, Function, and Antigenicity of the SARS-CoV-2 Spike Glycoprotein. *Cell* **2020**, *181*, 281−292.e6.
(40) Wang, Q.; Li, C.; Zhang, Q.; Wang, T.; Li, J.; Guan, W.; Yu, J.; Liang, M.; Li, D. Interactions of SARS coronavirus nucleocapsid protein with the host cell proteasome subunit p42. *Virol. J.* **2010**, *7*, 99.
(41) Thomas, S. The Structure of the Membrane Protein of SARS-CoV-2 Resembles the Sugar Transporter SemiSWEET. *Pathog. Immun.* **2020**, *5*, 342−363.
(42) Shrivastava, T.; Singh, B.; Rizvi, Z. A.; Verma, R.; Goswami, S.; Vishwakarma, P.; Jakhar, K.; Sonar, S.; Mani, S.; Bhattacharyya, S.; Awasthi, A.; Surjit, M. Comparative Immunomodulatory Evaluation of the Receptor Binding Domain of the SARS-CoV-2 Spike Protein; a Potential Vaccine Candidate Which Imparts Potent Humoral and Th1 Type Immune Response in a Mouse Model. *Front. Immunol.* **2021**, *12*, 641447.
(43) Armocida, D.; Palmieri, M.; Frati, A.; Santoro, A.; Pesce, A. How SARS-Cov-2 can involve the central nervous system. A systematic analysis of literature of the department of human neurosciences of Sapienza University, Italy. *J. Clin. Neurosci.* **2020**, *79*, 231−236.
(44) Chu, H.; Chan, J. F.; Yuen, T. T.; Shuai, H.; Yuan, S.; Wang, Y.; Hu, B.; Yip, C. C.; Tsang, J. O.; Huang, X.; Chai, Y.; Yang, D.; Hou, Y.; Chik, K. K.; Zhang, X.; Fung, A. Y.; Tsoi, H. W.; Cai, J. P.; Chan, W. M.; Ip, J. D.; Chu, A. W.; Zhou, J.; Lung, D. C.; Kok, K. H.; To, K. K.; Tsang, O. T.; Chan, K. H.; Yuen, K. Y. Comparative tropism, replication kinetics, and cell damage profiling of SARS-CoV-2 and SARS-CoV with implications for clinical manifestations, transmissibility, and laboratory studies of COVID-19: an observational study. *Lancet Microbe* **2020**, *1*, e14−e23.
(45) Shearer, L. J.; Petersen, N. O. Distribution and Co-localization of endosome markers in cells. *Heliyon* **2019**, *5*, No. e02375.
(46) Gonzalez-Jamett, A. M.; Momboisse, F.; Haro-Acuna, V.; Bevilacqua, J. A.; Caviedes, P.; Cardenas, A. M. Dynamin-2 function and dysfunction along the secretory pathway. *Front. Endocrinol.* **2013**, *4*, 126.
(47) Kalia, M.; Khasa, R.; Sharma, M.; Nain, M.; Vrati, S. Japanese encephalitis virus infects neuronal cells through a clathrin-independent endocytic mechanism. *J. Virol.* **2013**, *87*, 148−162.
(48) Bozym, R. A.; Morosky, S. A.; Kim, K. S.; Cherry, S.; Coyne, C. B. Release of intracellular calcium stores facilitates coxsackievirus entry into polarized endothelial cells. *PLoS Pathog.* **2010**, *6*, No. e1001135.
(49) Zhou, Y.; Frey, T. K.; Yang, J. J. Viral calciomics: interplays between Ca2+ and virus. *Cell Calcium* **2009**, *46*, 1−17.
(50) He, P.; Zou, Y.; Hu, Z. Advances in aluminum hydroxide-based adjuvant research and its mechanism. *Hum. Vaccines Immunother.* **2015**, *11*, 477−488.
(51) Ravichandran, S.; Coyle, E. M.; Klenow, L.; Tang, J.; Grubbs, G.; Liu, S.; Wang, T.; Golding, H.; Khurana, S. Antibody signature induced by SARS-CoV-2 spike protein immunogens in rabbits. *Sci. Transl. Med.* **2020**, *12*, eabc3539.
(52) Kannan, S. R.; Spratt, A. N.; Sharma, K.; Chand, H. S.; Byrareddy, S. N.; Singh, K. Omicron SARS-CoV-2 variant: Unique features and their impact on pre-existing antibodies. *J. Autoimmun.* **2022**, *126*, 102779.
(53) Cheng, S. M. S.; Mok, C. K. P.; Leung, Y. W. Y.; Ng, S. S.; Chan, K. C. K.; Ko, F. W.; Chen, C.; Yiu, K.; Lam, B. H. S.; Lau, E. H. Y.; Chan, K. K. P.; Luk, L. L. H.; Li, J. K. C.; Tsang, L. C. H.; Poon, L. L. M.; Hui, D. S. C.; Peiris, M. Neutralizing antibodies against the SARS-CoV-2 Omicron variant following homologous and heterologous CoronaVac or BNT162b2 vaccination. *Nat. Med.* **2022**, 486.
(54) Bolles, M.; Deming, D.; Long, K.; Agnihothram, S.; Whitmore, A.; Ferris, M.; Funkhouser, W.; Gralinski, L.; Totura, A.; Heise, M.;

https://doi.org/10.1021/acsinfecdis.2c00217
ACS Infect. Dis. XXXX, XXX, XXX−XXX

Baric, R. S. A double-inactivated severe acute respiratory syndrome coronavirus vaccine provides incomplete protection in mice and induces increased eosinophilic proinflammatory pulmonary response upon challenge. *J. Virol.* **2011**, *85*, 12201−12215.
(55) Yang, J.; Guertin, P.; Jia, G.; Lv, Z.; Yang, H.; Ju, D. Large-scale microcarrier culture of HEK293T cells and Vero cells in single-use bioreactors. *AMB Express* **2019**, *9*, 70.
(56) Tau, G.; Rothman, P. Biologic functions of the IFN-gamma receptors. *Allergy* **1999**, *54*, 1233−1251.
(57) Gadani, S. P.; Cronk, J. C.; Norris, G. T.; Kipnis, J. IL-4 in the brain: a cytokine to remember. *J. Immunol.* **2012**, *189*, 4213−4219.
(58) Xu, S.; Cao, X. Interleukin-17 and its expanding biological functions. *Cell. Mol. Immunol.* **2010**, *7*, 164−174.
(59) Desforges, M.; Le Coupanec, A.; Dubeau, P.; Bourgouin, A.; Lajoie, L.; Dube, M.; Talbot, P. J. Human Coronaviruses and Other Respiratory Viruses: Underestimated Opportunistic Pathogens of the Central Nervous System? *Viruses* **2020**, *12*, 14.
(60) Wu, Y.; Xu, X.; Chen, Z.; Duan, J.; Hashimoto, K.; Yang, L.; Liu, C.; Yang, C. Nervous system involvement after infection with COVID-19 and other coronaviruses. *Brain, Behav., Immun.* **2020**, *87*, 18−22.
(61) Bayati, A.; Kumar, R.; Francis, V.; McPherson, P. S. SARS-CoV-2 infects cells after viral entry via clathrin-mediated endocytosis. *J. Biol. Chem.* **2021**, *296*, 100306.
(62) Sanders, D. W.; Jumper, C. C.; Ackerman, P. J.; Bracha, D.; Donlic, A.; Kim, H.; Kenney, D.; Castello-Serrano, I.; Suzuki, S.; Tamura, T.; Tavares, A. H.; Saeed, M.; Holehouse, A. S.; Ploss, A.; Levental, I.; Douam, F.; Padera, R. F.; Levy, B. D.; Brangwynne, C. P. SARS-CoV-2 requires cholesterol for viral entry and pathological syncytia formation. *eLife* **2021**, *10*, e65962.
(63) Pang, H. B.; Braun, G. B.; Friman, T.; Aza-Blanc, P.; Ruidiaz, M. E.; Sugahara, K. N.; Teesalu, T.; Ruoslahti, E. An endocytosis pathway initiated through neuropilin-1 and regulated by nutrient availability. *Nat. Commun.* **2014**, *5*, 4904.
(64) Murugavelu, P.; Perween, R.; Shrivastava, T.; Singh, V.; Ahmad Parray, H.; Singh, S.; Chiranjivi, A. K.; Thiruvengadam, R.; Singh, S.; Yadav, N.; Jakhar, K.; Sonar, S.; Mani, S.; Bhattacharyya, S.; Sharma, C.; Vishwakarma, P.; Khatri, R.; Kumar Panchal, A.; Das, S.; Ahmed, S.; Samal, S.; Kshetrapal, P.; Bhatnagar, S.; Luthra, K.; Kumar, R. Non-neutralizing SARS CoV-2 directed polyclonal antibodies demonstrate cross-reactivity with the HA glycans of influenza virus. *Int. Immunopharmacol.* **2021**, *99*, 108020.
(65) Shrivastava, T.; Samal, S.; Tyagi, A. K.; Goswami, S.; Kumar, N.; Ozorowski, G.; Ward, A. B.; Chakrabarti, B. K. Envelope proteins of two HIV-1 clades induced different epitope-specific antibody response. *Vaccine* **2018**, *36*, 1627−1636.
(66) Parray, H. A.; Chiranjivi, A. K.; Asthana, S.; Yadav, N.; Shrivastava, T.; Mani, S.; Sharma, C.; Vishwakarma, P.; Das, S.; Pindari, K.; Sinha, S.; Samal, S.; Ahmed, S.; Kumar, R. Identification of an anti-SARS-CoV-2 receptor-binding domain-directed human monoclonal antibody from a naive semisynthetic library. *J. Biol. Chem.* **2020**, *295*, 12814−12821.

https://doi.org/10.1021/acsinfecdis.2c00217
ACS Infect. Dis. XXXX, XXX, XXX−XXX